Optical Materials 154 (2024) 115682

Contents lists available at ScienceDirect

Optical Materials

journal homepage: www.elsevier.com/locate/optmat

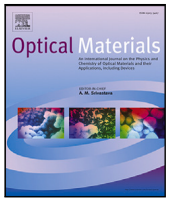

Research article

Switchable bi-functional water-based metasurface for high efficiency and wideband polarization conversion and absorption

Thi Quynh Hoa Nguyen [a,*], Huu Lam Phan [a], Thi Minh Nguyen [a], Ngoc Hieu Nguyen [b], Dac Tuyen Le [c], Xuan Khuyen Bui [d], Dinh Lam Vu [e], Jung-Mu Kim [f]

[a] School of Engineering and Technology, Vinh University, 182 Le Duan, Vinh city, 46000, Viet Nam
[b] Nghe An University of Economics, 51 Ly Tu Trong, Vinh city, 46000, Viet Nam
[c] Department of Physics, Hanoi University of Mining and Geology, 18 Pho Vien, Hanoi, 10000, Viet Nam
[d] Institute of Materials Sciences, Vietnam Academy of Science and Technology, 18 Hoang Quoc Viet, Hanoi, 10000, Viet Nam
[e] Graduate University of Science and Technology, Vietnam Academy of Science and Technology, 18 Hoang Quoc Viet, Hanoi, 10000, Viet Nam
[f] Department of Electronic Engineering, Jeonbuk National University, Jeonju, 54896, Republic of Korea

ARTICLE INFO

Keywords:
Water-based absorber
Metamaterials
Broadband
3D printing
Microwave

ABSTRACT

A reconfigurable metasurface with a switchable function, wideband, and high efficiency has gained a lot of attention for the creation of compact and efficient devices. Here, for the first time, we propose a bi-functional metasurface that utilizes a water-based resonator to achieve wideband and high-efficiency absorption and cross polarization conversion in the microwave range. By controlling the water injection, the functionality of the metasurface can switch between absorption and cross-polarized conversion. Via water injection, the designed water-based metasurface can act as a wideband absorber with an absorptivity of above 90% in the broadband range of 16.5–24 GHz. Meanwhile, without water injection, it exhibits the ability for high efficiency cross-polarization conversion across a wideband in the range of 4.38–11.9 GHz. The proposed metasurface is fabricated and measured to verify its ability to switch between the dual functions of high efficiency wideband absorption and cross-polarization conversion. We believe that the metasurface platform shown here will open up new possibilities for creating compact multifunctional devices for applications in the microwave region.

1. Introduction

Metasurfaces, two-dimensional (2D) metamaterials consisting of subwavelength features, have attracted considerable interest for fundamental research and promising device applications in the photonic and electronic fields. Owing to their unique features of ultrathin thickness, low weight, ease of fabrication, and high efficiency, various types of metasurfaces have applications in electromagnetic (EM) manipulation, including beam-steering devices [1,2], metalens [3–5], holograms [6], orbital angular momentums (OAMs) [7], metamirror [8], vortex beams [9], and ultrathin cloaks [10,11]. Recently, ultrathin metasurfaces have explored as a novel technique to control the polarization of EM waves that can replace conventional techniques using the Faraday Effect and the optical activity of crystals with the limitations of bulky size and narrow bandwidth [12]. In this regard, many cross-polarization conversion anisotropic metasurfaces with lightweight and wide bandwidth have been proposed [12–15].

Furthermore, the design of a perfect EM wave absorption based on metasurface has developed based on a metallic patterned layer and a ground plane sandwiched by a dielectric layer, which normally realizes a narrow bandwidth due to its resonant feature [16]. Therefore, many efforts have been proposed to enlarge the absorption bandwidth, especially in the microwave region for emerging applications, such as using the stack of metallic and dielectric [17,18] and lumped resistors [19–21]. Unfortunately, these approaches require a complex and expensive manufacturing process and there is a limitation for tuning the wideband absorption due to the complicated design of the metallic structure. Water is highly absorptive in the microwave regime, with a high value of the imaginary part of permittivity due to the hydrogen bonded network among water molecules [22,23], thus making it ideal for perfect wideband microwave absorption. The promising periodic dielectric water droplet-based perfect absorber is proposed [24], using the constitutive dispersive permittivity of water effectively. However, the large permittivity contrast between water and air, causes an impedance mismatch of the water film to free space, resulting in a large reflection of microwaves at the water–air interface and degrading the absorption function [23]. To overcome this drawback, a water container-based

* Corresponding author.
E-mail address: ntqhoa@vinhuni.edu.vn (T.Q.H. Nguyen).

https://doi.org/10.1016/j.optmat.2024.115682
Received 30 January 2024; Received in revised form 31 May 2024; Accepted 11 June 2024
Available online 15 June 2024

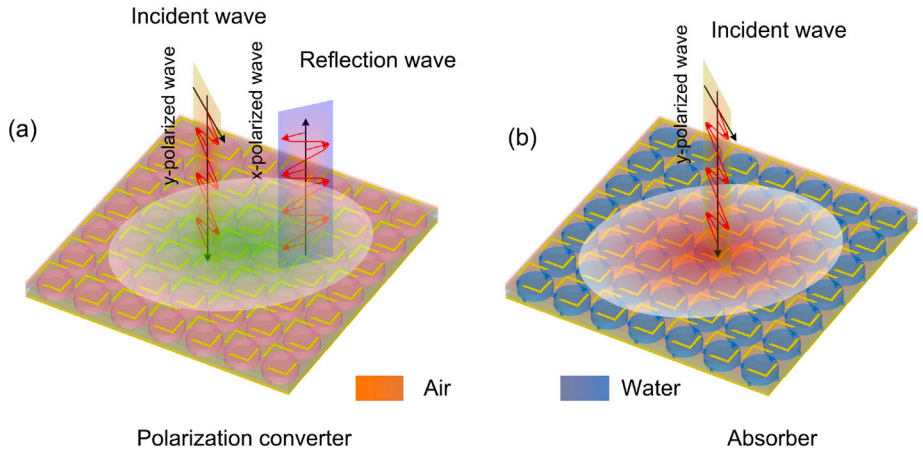

Fig. 1. Conceptual illustration of a microwave bifunctional metasurface that can switch its function from (a) polarization conversion to (b) perfect absorption by filling water.

metasurface has been explored to manipulate the impedance matching and deteriorate the reflection for perfect broadband absorption [23,25–28]. Due to the numerous advantages of water-based absorption structure, such as biocompatibility, optical transparency, and versatile tunability, it can be used in radar stealth, radiation prevention, and energy harvesting [29]. However, in view of device functions, most design approaches have limited to develop the metasurface structure with the single functionality of wideband absorption.

Recently, switchable and multi-functional metasurface manipulation strategies utilizing advanced materials such as graphene [30–32] and phase change material such as VO_2 [33–37] have been successfully developed to design multi-functional metasurfaces. However, these multi-functional metasurfaces can work in the THz region because of the large-scale production limitations of the material platform. Meanwhile, the design of microwave reconfigurable and multi-functional metasurfaces have been demonstrated based on the combination of lumped resistors and diodes [38–41]. However, these approaches are significantly complicated in both design and fabrication. Furthermore, they require maintaining a bias voltage source during use. Therefore, a facile approach to design of a microwave multi-functional metasurface is still a challenge for innovative applications.

In this work, we propose a switchable and broadband bi-functional metasurface for high efficiency absorption and polarization conversion using a water-resonator embedded in a metal/dielectric/metal configuration. We utilize water injection as an efficient and cost-effective approach to control the dielectric constant and, consequently, create a reconfiguration metasurface that can switch its functions from cross-polarization conversion to absorption with wideband and high efficiency. The low-cost fabrication and integration with dual functionalities make it a highly promising candidate for potential applications in the microwave range.

2. Design structure and method

To explore dual functions of absorption (ABS) and polarization conversion (PC) using metasurfaces in microwave region, firstly, we first design a cross-polarization converter using a metallic/dielectric/metallic configuration. To obtain the second function of absorption, in this design, a water container resonator is embedded with a FR4 layer to form a sandwich dielectric stack. It was reported that using a periodic water container structure instead of a continuous water layer, a variety of resonator modes in a water-based absorber structure at different operating frequencies can be excited to achieve wideband absorption [42–44]. Therefore, the water-based structure with water injection is used to obtain wideband absorption performance, while the water-resonator based on a cylindrical shape is chosen due to its insensitivity to polarization.

Fig. 1 displays the schematic of the proposed bi-functional microwave metasurface (BFMM) that can switch between PC and ABS modes by injecting pure water. The proposed structure of a unit cell consists of a metallic diagonal symmetrical pattern in the top layer, a dielectric layer that combines a FR4 substrate and a water container, and a metallic bottom layer, as shown in Fig. 2. The FR4 substrate has a dielectric constant of 4.3 and a loss tangent of 0.025. The metallic layers are made of copper with a conductivity of $\sigma = 4.56 \times 10^7$ S/m and a thickness of $t = 0.035$ mm. Meanwhile, the water container layer is designed using resin material (dielectric constant of 2.6 and loss tangent of 0.03). In order to make water channel between unit cells, the square channel of water (1 mm × 1 mm) is used. In this study, the full-wave simulation using commercial computer simulation technology (CST) Microwave Studio software is used to optimize and characterize the designed structure. In this simulation, the unit cell boundary conditions are applied to the x- and y-axis, while the open boundary condition is assigned to the z-axis. Furthermore, the pure water property is defined by the Debye model as follows [29,45,46]:

$$\epsilon(\omega) = \epsilon_\infty(\omega, T) + \frac{\epsilon_s(\omega, T) - \epsilon_\infty(\omega, T)}{1 - i\omega\tau(\omega, T)} \quad (1)$$

with temperature $T = 25$ °C, epsilon infinity $\epsilon_\infty = 3.1$, epsilon static $\epsilon_s(\omega, T) = 78.4$ and the relaxation time $\tau(\omega, T) = 8.27 \times 10^{-12}$ second.

Based on the aid of simulation method, the unit cell geometrical parameters of the BFMM are optimized as: $P = 16.4$ mm, $h_1 = 1$ mm, $h_2 = 1$ mm, $h_3 = 1.75$ mm, $h_4 = 1.25$ mm, $h_5 = 0.8$ mm; $S = 6.75$ mm; $w = 0.5$ mm; $c = 6.75$ mm, $D = 14$ mm, as depicted in Figs. 2(b) and (c), respectively.

When the container is filled with pure water, the BFMM structure operates in ABS mode. The cylindrical water container acts as the main resonator for absorption. To evaluate the performance of the ABS mode, the absorption ($A(\omega)$) can be expressed from the transmission ($T(\omega)$) and reflection ($R(\omega)$) coefficients as Eq. (2) [47,48]:

$$A(\omega) = 1 - R(\omega) - T(\omega), \quad (2)$$

where ω is the angular frequency, $R(\omega) = |r_{yy}|^2 + |r_{xy}|^2$, $T(\omega) = |t_{yy}|^2 + |t_{xy}|^2$, "$yy$", "$xy$" represent reflection, transmission, co-polarization, and cross-polarization components, respectively. Owing to the copper layer is deposited in the backside, T(ω) is zero. Therefore, the absorption is calculated through the reflective coefficient as: $A(\omega) = 1 - R(\omega)$.

In contrast, without water injection in the container, the BFMM structure works in PC mode. To evaluate the polarization conversion performance of a linear polarization converter, a polarization conversion ratio (PCR) is used that is calculated through the co- and cross-reflection coefficients. Assuming that the electric field of the incident wave is linearly polarized along the y-direction, PCR is expressed

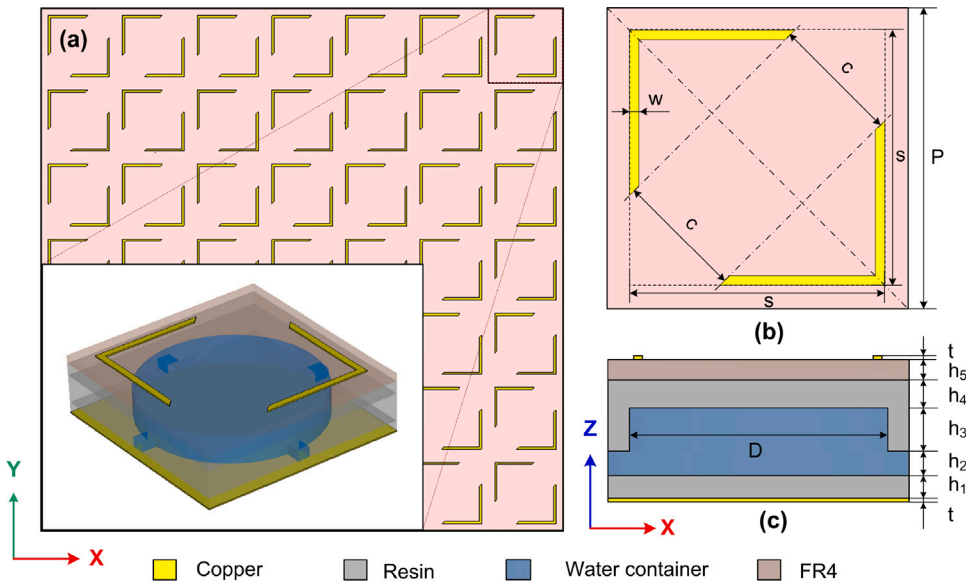

Fig. 2. The proposed bi-functional microwave metasurface: (a) the top-view and the inset is a magnified view of a 3D unit cell and (b) the top view and (c) the cross-section view of a unit cell.

as Eq. (3) [14,49].

$$PCR = \frac{|r_{xy}|^2}{|r_{xy}|^2 + |r_{yy}|^2} \tag{3}$$

where the co- and cross-reflection coefficients are defined as $r_{xy} = |E_{rx}|/|E_{iy}|$ and $r_{yy} = |E_{ry}|/|E_{iy}|$, with $|E_{rx}|$ and $|E_{ry}|$ are the magnitudes of the electric fields of the reflected wave components along the x- and y-axes, respectively.

In addition, the relative bandwidth (RBW) is used to evaluate the absorption and PCR performances, which is calculated as Eq. (4) [50].

$$RBW = 2 \times \frac{f_H - f_L}{f_H + f_L} \tag{4}$$

where f_H and f_L are the highest and lowest frequency of absorption range with absorption over 90%.

3. Results and discussion

3.1. The characteristics of the proposed BFMM operated for polarization conversion and absorption modes

Fig. 3 shows the simulation results of the proposed BFMM while the water container is filled with and without water. As seen in Fig. 3, without water filling, the proposed BFMM structure realizes fully cross-polarization conversion with PCR above 90% in the wideband from 4.38–11.9 GHz and RBW of 92.4% for normal incidence. Meanwhile, with full water filling, the proposed BFMM structure reveals a wideband absorption response with absorptivity higher than 90% in the range of 16.5–24 GHz. The simulated results indicate that the switchable bi-functions of the proposed metasurface for PC and ABS modes can be modulated by filling water.

To verify the operating ability of the water-based BFMM fabricated using various 3D printing resin materials, the BFMM performance for both PC and ABS modes is first investigated by changing the loss tangent and dielectric constant of the resin material in the range of 0.02 to 0.05 and 2.4 to 3.2, respectively, as shown in Figs. 4(a, b, d, e). As seen in Figs. 4(a) and (d), both PCR and ABS spectra are almost unchanged with the varying loss tangent of the resin in the range of 0.02–0.05. Furthermore, the absorption spectrum at the higher frequency shows a small red shift, while the efficiency of these spectra still stays as high as 90%, as shown in Figs. 4(b) and (e). These

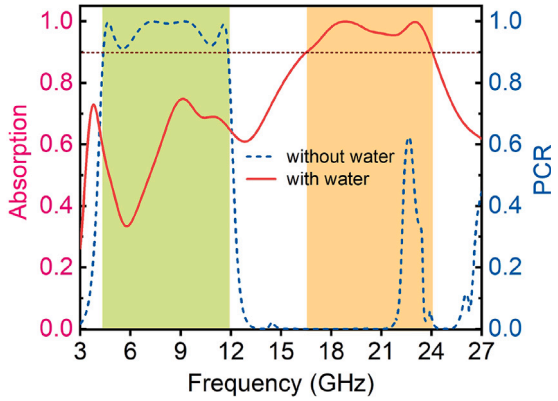

Fig. 3. The polarization conversion ratio and absorption spectra of the proposed BFMM without water and with water filling, respectively.

observations reveal that both the PCR and absorption spectra of water-based BFMM are not much changed by the large variation in the loss tangent and dielectric constant of the resin material. This could promise to fabricate water-based metasurfaces using commercial 3D resin materials.

Besides the effect of a resin material on the BFMM performance, a controllable operating frequency band is also demanded in many potential applications. Figs. 4(c) and (f) show the simulation results of the PCR and absorption spectra with different scaling of the unit cell dimension in the range of 0.6 to 1.4. By increasing the scaling from 0.6 to 1.4, both PCR and absorption spectra are shifted to lower frequencies, while these efficiencies and the RBW can remain almost unchanged. The detailed operating frequency band and the corresponding RBW of the proposed BFMM structure in both ABS and PC modes with varying scaling of unit cell dimensions are presented in Table 1. This design provides a convenient approach to controlling the operation frequency range by scaling its dimension.

3.2. Polarization conversion characteristics

Fig. 5 shows the magnitude and phase responses of the proposed BFMM structure without water injection. It is apparent that the magnitude of the cross-reflection coefficient is above 0.9 in a wide frequency

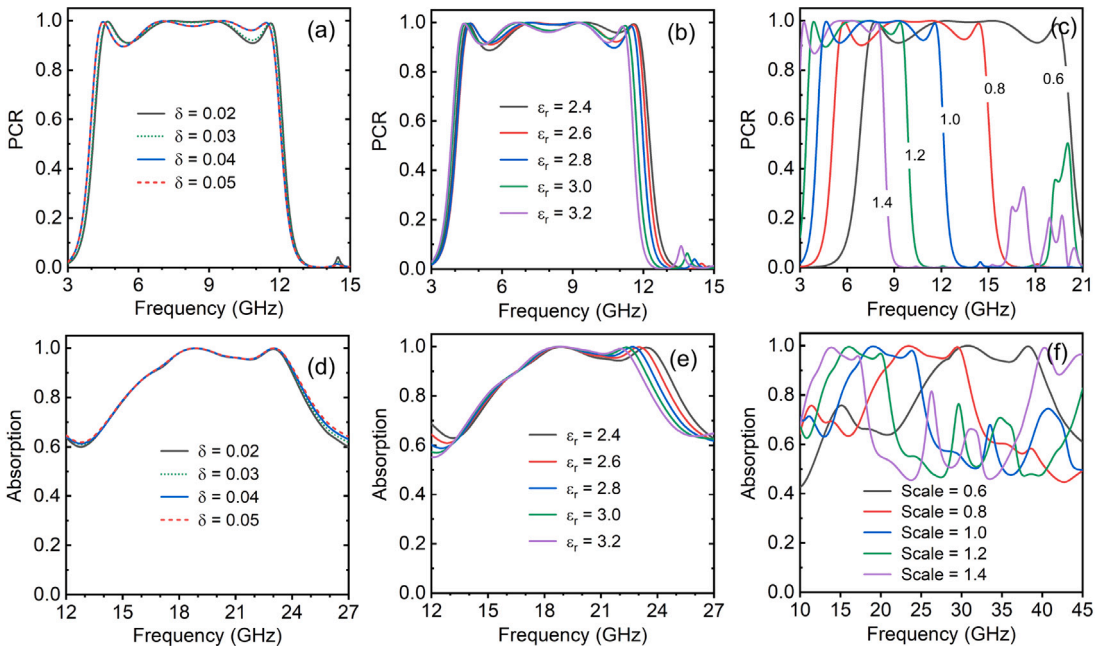

Fig. 4. The dependence of polarization conversion and absorption efficiencies as a function of the loss tangent and dielectric constant of the resin and the 3D structural scaling of the proposed BFMM operated at (a–c) polarization conversion and (d–f) absorption modes, respectively.

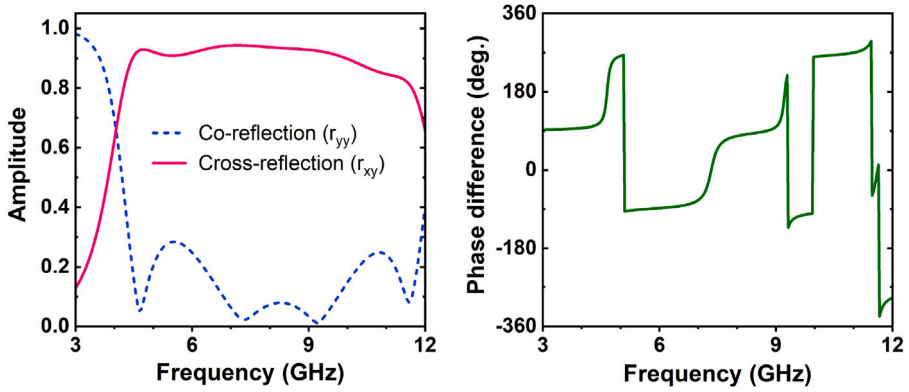

Fig. 5. The amplitude of co- and cross-reflection spectra and their phase difference.

Table 1
Performance of the proposed water-based BFMM with different scaling of the unit cell dimension.

Scale	PC mode		ABS mode	
	Working band with PCR > 90% (GHz)	RBW (%)	Working band with absorptivity > 90% (GHz)	RBW (%)
0.6	7.31–19.8	92.06	26.64–39.89	39.83
0.8	5.45–14.75	92.07	20.44–30.54	39.62
1	4.38–11.9	92.38	16.5–24	37.03
1.2	3.63–9.62	90.41	13.99–20.58	38.12
1.4	3.06–8.15	90.81	12.21–17.66	36.49

range from 4.38 GHz to 11.9 GHz. Conversely, within that working band, the co-reflection factor is below 0.285. Furthermore, the four min peaks of the co-reflection are observed at 4.6 GHz, 7.3 GHz, 9.2 GHz, and 11.8 GHz with values of 0.05, 0.02, 0.01, and 0.08, respectively. It suggests that the combination of these strong resonances created at the aforementioned frequencies contributes to the wideband polarization conversion feature. The phase difference between the phase of the co- and the cross-polarization coefficient is $90° \times n$ or $-90° \times n$ (n is an odd integer) in the working band of 4.38–11.9 GHz. It confirms that the proposed structure exhibits the cross-polarization conversion (CPC) across a wide frequency range.

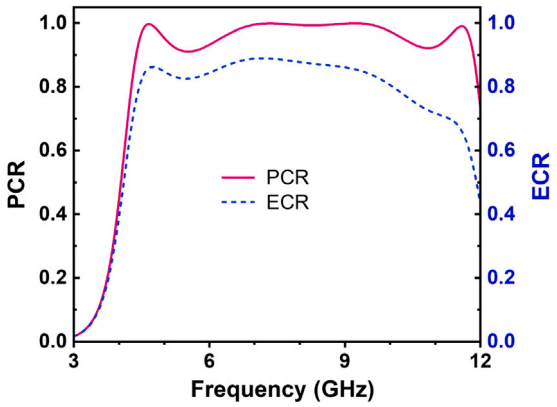

Fig. 6. PCR and ECR spectra of the proposed BFMM operated at polarization conversion mode (without water filling).

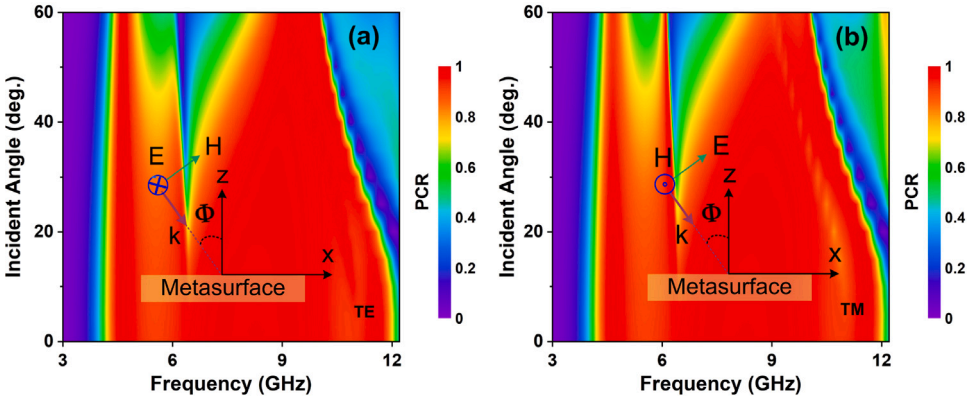

Fig. 7. The dependence of PCR as a function of incident angle under (a) TE and (b) TM modes.

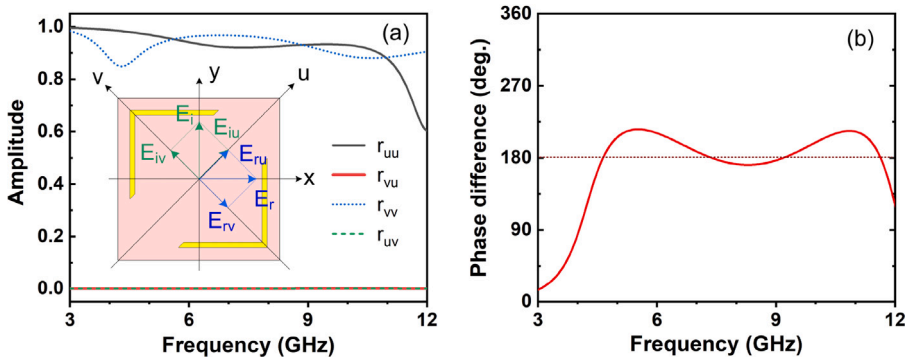

Fig. 8. (a) The reflection magnitude spectra and (b) phase difference in u- and v-directions.

The PCR is used to evaluate the efficiency of linear polarization conversion concerning the reflection wave (the co- and cross-polarized reflection waves), as shown in Eq. (3). To further comprehend the purity of converted component, we define another parameter called the energy conversion ratio (ECR) of cross-polarization reflection power and overall energy [51]. For y-polarized incident wave, the ECR is given by $\mathrm{ECR}=|E_{rx}|^2/|E_{iy}|^2 = \left|r_{xy}\right|^2$. Fig. 6 shows the PCR and ECR of the proposed BFMM operated at PC mode. The ECR value is lower than the PCR value. However, the ECR is kept above 0.8 in the range of 4.3–10 GHz. It indicates that the EM incident wave is partially absorbed in the BFMM structure.

To evaluate the polarization conversion performance of the proposed BFMM structure without water injection, we investigate its polarization conversion under various oblique incident angles for both transverse electric (TE) and transverse magnetic (TM) modes. Fig. 7 shows the simulated PCR map as a function of the incident angles for both TE and TM modes. With increasing the incident angle, the bandwidth of the proposed BFMM structure shrinks for both modes. It is attributed to the destructive interference at the surface of the metasurface structure [52]. Furthermore, there is a dip that occurred at around 6.5 GHz for both modes, which is due to strong absorption at this frequency [15,52]. However, our structure can maintain PCR efficiency as high as 80% in the bands from 4.38 to 6.3 GHz and 6.7 to 11 GHz with an incident angle up to 40°. This obtained result proves that the proposed BFMM structure exhibits a stable polarization conversion with a wide range of incidence angles.

To explain the working principle of the polarization conversion of the proposed BFMM, we simulate the amplitude and phase difference of the reflection coefficients, and these results are shown in Figs. 8 (a) and (b). Assuming that the incident wave is polarized along the y-axis, it is analyzed into two orthogonal components along the u- and v-axes. These u and v axes rotate around the y-axis by ±45°, respectively. Hence, the incident electric field E_i and reflected electric field E_r of the EM wave can be expressed as:

$$E_i = E_{iu} + E_{iv} \tag{5}$$

$$E_r = E_{ru} + E_{rv} = r_{uu}E_{iu} + r_{vv}E_{iv} \tag{6}$$

where r_{uu} and r_{vv} are the reflected coefficients along the u-axis and v-axis, which can be defined as $r_{uu} = |E_{ru}|/|E_{iu}|$, and $r_{uu} = |E_{rv}|/|E_{iv}|$. Here, the energy loss of the incident EM waves can be neglected because of a low-loss dielectric. Therefore, the amplitudes of r_{uu} and r_{vv} can be assumed to be equal unity ($|r_{uu}| = |r_{vv}| = 1$). Furthermore, due to the asymmetrical structure of the BFMM structure, there is a phase difference ($\Delta\varphi$) between r_{uu} and r_{vv} [52]. The relation between r_{uu} and r_{vv} can be given by: $r_{vv} = r_{uu}e^{j\Delta\varphi}$. Therefore, Eq. (6) can be represented as Eq. (7):

$$E_r = r_{uu}E_{iu} + r_{uu}e^{j\Delta\varphi}E_{iv} \tag{7}$$

When $|\Delta\varphi| = 180° + 2k\pi$ (k is an integer), the reflected electric fields in the uv-axis direction are $E_{ru} = r_{uu}E_{iu}$ and $E_{rv} = -r_{uu}E_{iv}$. It implies that E_{ru} or E_{rv} is opposite to their respective incident direction, resulting in the synthetic reflected electric field (E_r) is rotated exactly 90° in relation to the incidence, as depicted in the inset of Fig. 8(a). To confirm this analysis, the magnitude and phase difference of the reflections for u- and v-polarized incident waves under normal incidence is simulated. As illustrated in Fig. 8(a), the amplitude of the co-polarized reflections (r_{uu} and r_{vv}) and cross-polarized reflections (r_{vu} and r_{uv} are nearly equal to 1 and 0 in the wideband from 4.38 to 11.9 GHz, respectively. Furthermore, Fig. 8(b) illustrates the phase difference $\Delta\varphi$ between r_{uv} and r_{vu} from 4.38 GHz to 11.9 GHz is $180° - 35° \le \Delta\varphi \le 180° + 35°$. The phase difference is equal to 180° at 4.6 GHz, 7.3 GHz, 9.2 GHz, and 11.8 GHz, which is the same as with four resonant frequencies of the polarization converter. These

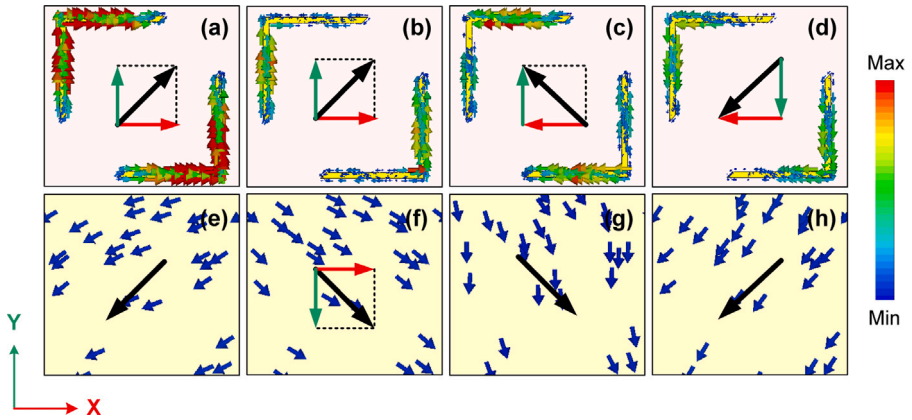

Fig. 9. Surface current distributions on (a–d) top metallic layer and (e–h) ground metallic layer in a unit-cell of the proposed BFMM at various resonant frequencies of 4.6 GHz, 7.3 GHz, 9.2 GHz, and 11.8 GHz, respectively.

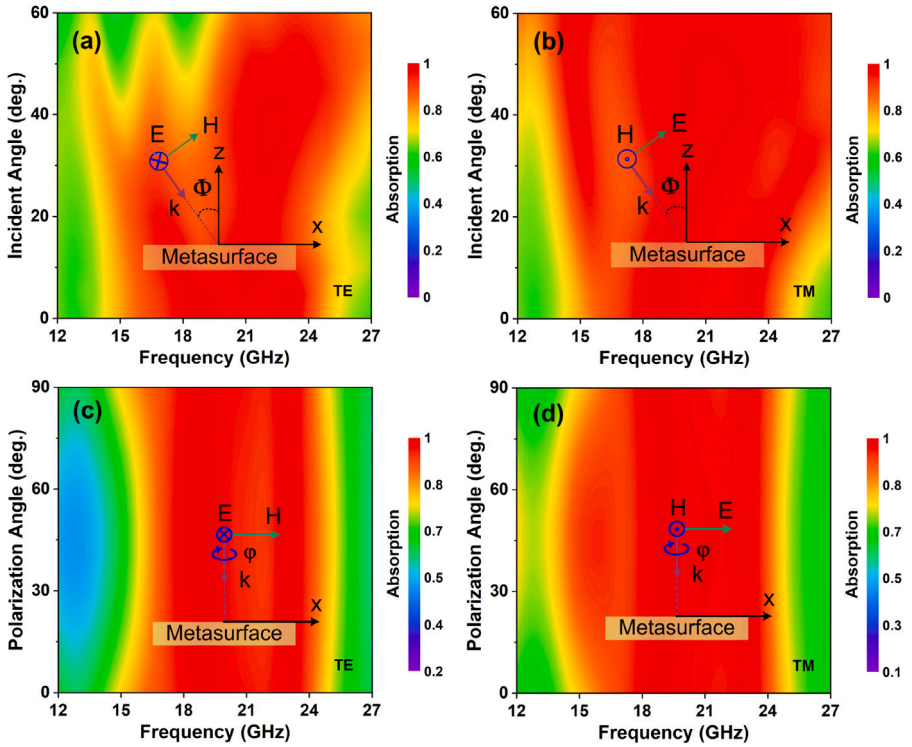

Fig. 10. The dependence of absorption efficiency as a function of (a, b) incident angle and (c, d) polarization angle under TE and TM modes, respectively.

results confirm that the cross-polarization conversion characteristic in the wideband of the BFMM structure without water injection.

To gain insight into the physical mechanism of the CPC performance of the proposed BFMM structure, the surface current distributions are analyzed at the four resonant frequencies of 4.6 GHz, 7.3 GHz, 9.2 GHz, and 11.8 GHz (Fig. 9). The black-colored arrows represent the synthesized surface current direction of each layer. As shown in Figs. 9(a), (e) and Figs. 9(c), (g), the surface currents on the top layer and ground layer are anti-parallel at the frequencies of 4.6 GHz and 9.2 GHz, which is due to magnetic resonance [53]. On the contrary, at the resonant frequency of 11.8 GHz, the surface currents on the top layer are parallel to those on the ground layer, which is contributed by electric resonance (Figs. 9(d), (h)) [15,54]. At the frequency of 7.3 GHz, the top and ground surface currents in the y- and x-axes are anti-parallel and parallel, respectively, as illustrated in Figs. 9(b) and (f). It implies that the resonant frequency of 7.3 GHz is originated from magnetic resonance associated with electric resonance [14].

3.3. Absorption characteristics

Figs. 10(a) and (b) present the absorption performance of the proposed BFMM structure with full water injection under various incident angles for the TE and TM modes, respectively. It can be seen that the proposed structure can achieve an absorption rate of above 80% for both TE and TM modes when increasing the incident angle until $\theta = 35°$. However, with further increasing the incident angle in the TE mode, the bandwidth of the suggested structure decreases substantially, as shown in Fig. 10(a). Meanwhile, the absorption intensity of the proposed structure is unaffected by changing the incident angle in the TM mode. It is still maintained above 85% in the interested bands, as depicted in Fig. 10(b). It was reported that the observation of high absorption efficiency with large incident angles in the TM mode is owing to magnetic field orientation [55]. Furthermore, the proposed structure can work stable under different polarization angles. Figs. 10(c) and (d) illustrate that the absorption intensities are identical at various

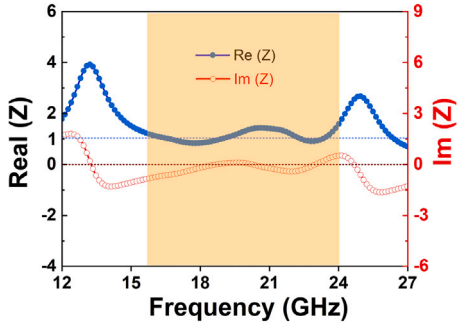

Fig. 11. The normalized impedance spectrum of the proposed bi-function metasurface operated at absorption mode.

polarization angles under normal incidence for TE and TM modes. It proves that the proposed structure has a polarization-insensitive characteristic due to its symmetry structure.

When the perfect impedance matching between the free space and the BFMM structure occurs, the reflection coefficient will be zero and the perfect absorption will be obtained. To determine impedance matching, the normalized input impedance (Z(ω)) of the BFMM is calculated based on the effective medium interference theory, given by Eq. (8) [47,56].

$$Z(\omega) = \sqrt{\frac{(1+S_{11})^2 - S_{21}^2}{(1-S_{11})^2 - S_{21}^2}} = \frac{1+S_{11}}{1-S_{11}} \tag{8}$$

As seen in Fig. 11, the real and imaginary components of the normalized impedance are pretty close to 1 and 0, respectively, in the frequency range from 16.5 to 24 GHz. It is evident that good impedance matching between the proposed BFMM structure and free space in the wide band is obtained, leading to near-perfect wideband absorption, as presented in Fig. 3. Furthermore, the power loss density at various resonant frequencies of 18.8 GHz and 23 GHz is illustrated in Fig. 12. It can be seen that the power of the incident wave is mainly absorbed by the water resonator at different frequencies of 18.8 GHz and 23 GHz. The power loss at 18.8 GHz is lost on both the top and bottom surfaces of the cylindrical water layer. At 23 GHz, the power loss mainly occurs at the interface between the top surface of the water layer and the resin container. This can be explained by the dielectric resonator mode [29,57,58]. With the fixed dimensions of the water resonator, the resonant frequency for a particular mode in the resonator can be considered as having a linear relationship with its electrical size, which can be found using the formula $f = \lambda/\sqrt{\epsilon}$, where λ is the wavelength in free space. According to the Debye model, ϵ decreases with frequency, causing the electrical size of the resonator to vary a small amount across a wide frequency band. This characteristic enables the dielectric resonance mode to be maintained across a wide band. Therefore, the varying dielectric constant of water can ignore the influence induced by the varying electrical size of the resonator with frequency [57,58].

3.4. Experimental verification

To verify the simulation results of the proposed BFMM structure, a sample structure containing 12 × 12 unit cells (an overall size of 198.8 mm × 198.8 mm) has been fabricated with the designed parameters, as illustrated in Fig. 13. As can be seen in Fig. 13(a), the split-square patterns are patterned on an FR4 substrate with a thickness of 0.8 mm by a conventional printed circuit board process. Meanwhile, the water container is made from a 3D printing machine using Polylactic Acid (PLA) resin, as shown in Fig. 13(b). In addition, Fig. 13(c) displays the copper bottom layer and 3D view of the fabricated sample. The measurement setup for the fabricated structure was presented in the previous study [15], which uses two identical linearly polarized standard gain horn antennas connected to a vector network analyzer (Rohde and Schwarz ZNB20). One horn antenna is responsible for transmitting vertical or horizontal-polarized waves, while the remaining one receives vertical and horizontal polarized waves. Furthermore, the spacing angle between two antennas is calibrated to correspond to the normal incidence measurement in the experimental setup. Owing to the limitations of our VNA instrument range below 18 GHz, the measurement data is gathered in the range of 2–18 GHz. Figs. 13(d) and (e) show the simulated and measured results of PCR and absorption spectra of the proposed BFMM structure in the cases of without and with water injection, respectively. It is evident that there is a good correlation between the simulation and the experimental results. Errors in system alignment, fabrication imperfections, and limitations of the fabricated dimension are some of the experimental factors that are responsible for the slight difference between simulation and measurement [52].

Table 2 illustrates the performance comparison of the proposed structure with the existing switchable microwave metasurfaces, which were recently reported in the literature. The comparison is implemented in terms of the operation mode, working frequency band, relative bandwidth, and switching mechanism. As seen in Table 2, the proposed structure can operate in the wide bandwidth with the switchable dual function of polarization conversion or absorption. Compared with the metasurfaces with similar dual functions in [39], the studied one shows a narrower BW in ABS mode, but is higher than in PC mode. Moreover, reported in [39] required complex and expensive fabrication due to the need for electronic components and power supply for bias voltage, which might be considered as effective of our design.

4. Conclusion

A wideband and high-efficiency switchable bi-functional water-based metasurface in the microwave region was proposed. A water-container resonator was embedded inside the metal/dielectric/metal configuration to obtain a switchable metasurface with dual functions, including absorption or cross-polarization conversion, by tailoring the water injection. The designed metasurface, when filled with water, can act as a wideband absorber with an absorptivity of more than 90% in the broadband range of 16.5–24 GHz. Meanwhile, even without water, it can perform high-efficiency cross-polarization conversion across a wideband of 4.38–11.9 GHz. The proposed metasurface was fabricated and measured and a good agreement between simulation and

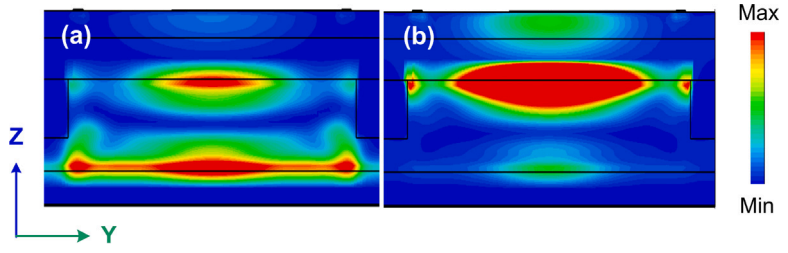

Fig. 12. The cross-section power loss density at various resonant frequencies of (a) 18.8 GHz and (b) 23 GHz.

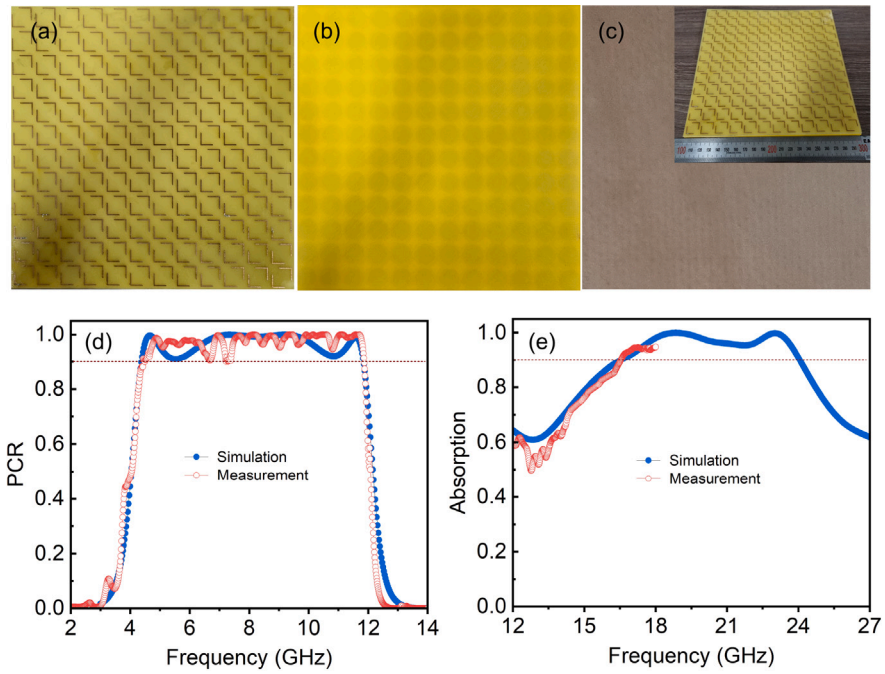

Fig. 13. The photograph of the fabricated sample: (a) top view of the metal layer for PC mode, (b) top view of the water container for ABS mode, and (c) bottom Cu ground layer and its inset is a 3D view of the fabricated sample. The simulated and measured results of the fabricated structure: (d) PCR (without water injection) and (e) absorption spectra (with full water injection).

Table 2
Performance of the proposed switchable bi-functional microwave metasurface and existing works in literature.

Refs.	Operation mode	Working band (GHz)	RBW (%)	Switching mechanism
[59]	ABS PC	4.48 &10.54& 21.02 14.43–20.32	NA 33.9	Mechanical method
[60]	ABS Reflection	8.0–22.0 8.0–22.0	93.3 93.3	Thermal method
[61]	ABS PC	5.4 5.4	NA NA	Electrical method
[39]	ABS PC	2.56–7.62 2.97–6.03	99.4 68.0	Electrical method
[62]	ABS PC	16.1–16.9 5.9–10 & 14.3–16.4	4.8 51.5 & 13.7	Water-based method
This work	ABS PC	16.5–24 4.38–11.9	37 92.4	Water-based method

measurement was achieved. It was possible to control the operating frequency band of the water-based BFMM design according to the scale of its dimensions and print with various resin materials. We believe that the metasurface platform shown here will open up new avenues for developing compact multifunctional devices for microwave applications.

CRediT authorship contribution statement

Thi Quynh Hoa Nguyen: Writing – review & editing, Writing – original draft, Supervision, Investigation, Conceptualization. **Huu Lam Phan:** Investigation, Formal analysis, Data curation. **Thi Minh Nguyen:** Investigation, Formal analysis, Data curation. **Ngoc Hieu Nguyen:** Writing – review & editing, Investigation, Formal analysis, Data curation. **Dac Tuyen Le:** Writing – review & editing, Investigation, Formal analysis, Data curation. **Xuan Khuyen Bui:** Writing – review & editing, Investigation, Formal analysis, Data curation. **Dinh Lam Vu:** Writing – review & editing, Software. **Jung-Mu Kim:** Writing – review & editing, Investigation, Formal analysis, Data curation.

Declaration of competing interest

The authors declare that they have no known competing financial interests or personal relationships that could have appeared to influence the work reported in this paper.

Data availability

No data was used for the research described in the article.

Acknowledgments

This research is funded by Vietnam National Foundation for Science and Technology Development (NAFOSTED) under grant number 103.02-2021.44.

References

[1] Z. Wei, Y. Cao, X. Su, Z. Gong, Y. Long, H. Li, Highly efficient beam steering with a transparent metasurface, Opt. Express 21 (9) (2013) 10739–10745.

[2] J. Wu, Z. Shen, S. Ge, B. Chen, Z. Shen, T. Wang, C. Zhang, W. Hu, K. Fan, W. Padilla, Y. Lu, B. Jin, J. Chen, P. Wu, Liquid crystal programmable metasurface for terahertz beam steering, Appl. Phys. Lett. 116 (13) (2020) 131104.

[3] Q. Wang, X. Zhang, Y. Xu, Z. Tian, J. Gu, W. Yue, S. Zhang, J. Han, W. Zhang, A broadband metasurface-based terahertz flat-lens array, Adv. Opt. Mater. 3 (6) (2015) 779–785.

[4] C. Li, Z. Song, Tailoring terahertz wavefront with state switching in VO2 Pancharatnam–Berry metasurfaces, Opt. Laser Technol. 157 (2023) 108764.

[5] R. Nie, C. He, R. Zhang, Z. Song, Vanadium dioxide-based terahertz metasurfaces for manipulating wavefronts with switchable polarization, Opt. Laser Technol. 159 (2023) 109010.

[6] Z. Du, C. He, J. Xin, Z. Song, Terahertz dynamic multichannel holograms generated by spin-multiplexing reflective metasurface, Opt. Express 32 (1) (2024) 248–259, http://dx.doi.org/10.1364/OE.510046.

[7] K. Guo, M. Zhang, Z. Du, Z. Song, Terahertz spin-selective metasurface for multichannel switching of OAM, Results Phys. 56 (2024) 107279.

[8] J. Xu, W. Liu, Z. Song, Graphene-based terahertz metamirror with wavefront reconfiguration, Opt. Express 29 (24) (2021) 39574–39585.

[9] Z. Zhou, Z. Song, Terahertz mode switching of spin reflection and vortex beams based on graphene metasurfaces, Opt. Laser Technol. 153 (2022) 108278.

[10] X. Ni, Z.J. Wong, M. Mrejen, Y. Wang, X. Zhang, An ultrathin invisibility skin cloak for visible light, Science 349 (6254) (2015) 1310–1314.

[11] H.-X. Xu, G. Hu, Y. Wang, C. Wang, M. Wang, S. Wang, Y. Huang, P. Genevet, W. Huang, C.-W. Qiu, Polarization-insensitive 3D conformal-skin metasurface cloak, Light Sci. Appl. 10 (1) (2021).

[12] M.I. Khan, Z. Khalid, F.A. Tahir, Linear and circular-polarization conversion in X-band using anisotropic metasurface, Sci. Rep. 9 (1) (2019).

[13] M.I. Khan, Q. Fraz, F.A. Tahir, Ultra-wideband cross polarization conversion metasurface insensitive to incidence angle, J. Appl. Phys. 121 (4) (2017) 045103.

[14] T.N. Cao, M.T. Nguyen, N.H. Nguyen, C.L. Truong, T.Q.H. Nguyen, Numerical design of a high efficiency and ultra-broadband terahertz cross-polarization converter, Mater. Res. Exp. 8 (6) (2021) 065801.

[15] T.M. Nguyen, T.K.T. Nguyen, D.T. Phan, D.T. Le, D.L. Vu, T.Q.H. Nguyen, J.-M. Kim, Ultra-wideband and lightweight electromagnetic polarization converter based on multiresonant metasurface, IEEE Access 10 (2022) 92097–92104.

[16] J. Zhu, Z. Ma, W. Sun, F. Ding, Q. He, L. Zhou, Y. Ma, Ultra-broadband terahertz metamaterial absorber, Appl. Phys. Lett. 105 (2) (2014) 021102.

[17] F. Ding, Y. Cui, X. Ge, Y. Jin, S. He, Ultra-broadband microwave metamaterial absorber, Appl. Phys. Lett. 100 (10) (2012).

[18] N. Thi Quynh Hoa, P. Huu Lam, P. Duy Tung, Wide-angle and polarization-independent broadband microwave metamaterial absorber, Microw. Opt. Technol. Lett. 59 (5) (2017) 1157–1161.

[19] D. Kundu, A. Mohan, A. Chakrabarty, Single-layer wideband microwave absorber using array of crossed dipoles, IEEE Antennas Wirel. Propag. Lett. 15 (2016) 1589–1592.

[20] T.T. Nguyen, S. Lim, Angle- and polarization-insensitive broadband metamaterial absorber using resistive fan-shaped resonators, Appl. Phys. Lett. 112 (2) (2018) 021605.

[21] D.T. Phan, T.K.T. Nguyen, N.H. Nguyen, D.T. Le, X.K. Bui, D.L. Vu, C.L. Truong, T.Q.H. Nguyen, Lightweight, ultra-wideband, and polarization-insensitive metamaterial absorber using a multilayer dielectric structure for C- and X-Band applications, Phys. Status Solidi b 258 (10) (2021) 2100175.

[22] R. Buchner, J. Barthel, J. Stauber, The dielectric relaxation of water between 0°C and 35°C, Chem. Phys. Lett. 306 (1) (1999) 57–63.

[23] Q. Song, W. Zhang, P.C. Wu, W. Zhu, Z.X. Shen, P.H.J. Chong, Q.X. Liang, Z.C. Yang, Y.L. Hao, H. Cai, H.F. Zhou, Y. Gu, G.-Q. Lo, D.P. Tsai, T. Bourouina, Y. Leprince-Wang, A.-Q. Liu, Water-resonator-based metasurface: An ultrabroadband and near-unity absorption, Adv. Opt. Mater. 5 (8) (2017) 1601103.

[24] Y.J. Yoo, S. Ju, S.Y. Park, Y.J. Kim, J. Bong, T. Lim, K.W. Kim, J.Y. Rhee, Y. Lee, Metamaterial absorber for electromagnetic waves in periodic water droplets, Sci. Rep. 5 (1) (2015).

[25] J. Xie, W. Zhu, I.D. Rukhlenko, F. Xiao, C. He, J. Geng, X. Liang, R. Jin, M. Premaratne, Water metamaterial for ultra-broadband and wide-angle absorption, Opt. Express 26 (4) (2018) 5052–5059.

[26] H. Xiong, F. Yang, Ultra-broadband and tunable saline water-based absorber in microwave regime, Opt. Express 28 (4) (2020) 5306–5316.

[27] Q. Wu, F. Ling, C. Zhang, Z. Zhong, B. Zhang, Water-based metamaterials absorber with broadband absorption in terahertz region, Opt. Commun. 526 (2023) 128874.

[28] H.L. Phan, D.T. Le, X.K. Bui, D.L. Vu, H.Q. Nguyen, N.H. Duong, T.M. Nguyen, T.Q.H. Nguyen, J.-M. Kim, High efficiency and ultra-wideband water-based microwave absorber using 3D printing, Opt. Commun. 556 (2024) 130297.

[29] J. Wen, Q. Zhao, R. Peng, H. Yao, Y. Qing, J. Yin, Q. Ren, Progress in water-based metamaterial absorbers: a review, Opt. Mater. Express 12 (4) (2022) 1461.

[30] M. Barkabian, N. Sharifi, N. Granpayeh, Multi-functional high-efficiency reflective polarization converter based on an ultra-thin graphene metasurface in the THz band, Opt. Express 29 (13) (2021) 20160–20174.

[31] Z. Li, R. Yang, J. Wang, Y. Zhao, J. Tian, W. Zhang, Multifunctional metasurface for broadband absorption, linear and circular polarization conversions, Opt. Mater. Express 11 (10) (2021) 3507–3519.

[32] Q. Xie, J. Sun, C. Su, F. Xia, M. Wang, K. Zhang, M. Yun, Multifunctional metasurface for broadband absorption and polarization conversion based on graphene-VO2, Diam. Relat. Mater. 137 (2023) 110119.

[33] F. Ding, S. Zhong, S.I. Bozhevolnyi, Vanadium dioxide integrated metasurfaces with switchable functionalities at terahertz frequencies, Adv. Opt. Mater. 6 (9) (2018) 1701204.

[34] Y. Zhao, R. Yang, Y. Wang, W. Zhang, J. Tian, VO2-assisted multifunctional metamaterial for polarization conversion and asymmetric transmission, Opt. Express 30 (15) (2022) 27407–27417.

[35] T.M. Nguyen, D.L. Vu, T.Q.H. Nguyen, J.-M. Kim, Reconfigurable broadband metasurfaces with nearly perfect absorption and high efficiency polarization conversion in THz range, Sci. Rep. 12 (1) (2022).

[36] Y. Sun, Y. Wang, H. Ye, J. Li, H. Fan, L. Yu, Z. Yu, Y. Liu, T. Wu, Switchable bi-functional metasurface based on VO2 for ultra-broadband polarization conversion and perfect absorption in same infrared waveband, Opt. Commun. 503 (2022) 127442.

[37] H.L. Phan, T.Q.H. Nguyen, J.-M. Kim, Multi-functional wideband metasurface: Perfect absorber and linear to linear and linear to circular polarization converter, IEEE Access 12 (2024) 11664–11673.

[38] R. Dutta, D. Mitra, J. Ghosh, Dual-band multifunctional metasurface for absorption and polarization conversion, Int. J. RF Microw. Comput. Aided Eng. 30 (7) (2020) e22200.

[39] J. Wang, R. Yang, R. Ma, J. Tian, W. Zhang, Reconfigurable multifunctional metasurface for broadband polarization conversion and perfect absorption, IEEE Access 8 (2020) 105815–105823.

[40] Y. Li, H. Li, Y. Wang, Y. Wang, Q. Cao, A novel switchable absorber/linear converter based on active metasurface and its application, IEEE Trans. Antennas and Propagation 68 (11) (2020) 7688–7693.

[41] H.L. Wang, H.F. Ma, M. Chen, S. Sun, T.J. Cui, A reconfigurable multifunctional metasurface for full-space control of electromagnetic waves, Adv. Funct. Mater. 31 (25) (2021) 2100275.

[42] X. Zhang, F. Yan, X. Du, W. Wang, M. Zhang, Broadband water-based metamaterial absorber with wide angle and thermal stability, AIP Adv. 10 (5) (2020) 055211.

[43] Y. Lu, J. Chen, J. Li, Design of all-dielectric ultra-wideband transparent water-based absorber, J. Phys. D: Appl. Phys. 55 (11) (2021) 115502.

[44] L. Du, T. Shi, S. Dong, X. Wang, M. Zhou, J. Zhao, X. Huang, Ultra broadband microwave metamaterial absorber with multiple strong absorption peaks induced by sandwiched water resonators, Appl. Phys. A 128 (10) (2022) 864.

[45] Y. Shen, J. Zhang, Y. Pang, L. Zheng, J. Wang, H. Ma, S. Qu, Thermally tunable ultra-wideband metamaterial absorbers based on three-dimensional water-substrate construction, Sci. Rep. 8 (1) (2018).

[46] X. Yan, X. Kong, Q. Wang, L. Xing, F. Xue, Y. Xu, S. Jiang, X. Liu, Water-based reconfigurable frequency selective rasorber with thermally tunable absorption band, IEEE Trans. Antennas Propag. 68 (8) (2020) 6162–6171.

[47] S. Bhattacharyya, K. Vaibhav Srivastava, Triple band polarization-independent ultra-thin metamaterial absorber using electric field-driven LC resonator, J. Appl. Phys. 115 (6) (2014) 064508.

[48] T.K.T. Nguyen, T.N. Cao, N.H. Nguyen, L.D. Tuyen, X.K. Bui, C.L. Truong, D.L. Vu, T.Q.H. Nguyen, Simple design of a wideband and wide-angle insensitive metamaterial absorber using lumped resistors for X- and Ku-bands, IEEE Photonics J. 13 (3) (2021) 1–10.

[49] T.M. Nguyen, H.L. Phan, D.L. Vu, T.Q.H. Nguyen, J.-M. Kim, Ultra-wideband and high-efficiency cross-polarization conversion using a double split ring shaped metasurface for C, X, and Ku-band applications, AIP Adv. 12 (11) (2022).

[50] T.Q.M. Nguyen, T.K.T. Nguyen, D.T. Le, C.L. Truong, D.L. Vu, T.Q.H. Nguyen, Numerical study of an ultra-broadband and wide-angle insensitive perfect metamaterial absorber in the UV–NIR region, Plasmonics 16 (5) (2021) 1583–1592.

[51] M. Yang, F. Lan, Y. Zhang, L. Qi, G. He, Y. Pan, T. Song, L. Wang, P. Mazumder, H. Zeng, Z. Yang, Collective-coupling enhanced ultrabroadband linear polarization conversion on zigzag-split metasurfaces, IEEE Trans. Antennas and Propagation 71 (6) (2023) 5001–5013.

[52] J. Xu, R. Li, J. Qin, S. Wang, T. Han, Ultra-broadband wide-angle linear polarization converter based on H-shaped metasurface, Opt. Express 26 (16) (2018) 20913.

[53] D. Neshev, I. Aharonovich, Optical metasurfaces: new generation building blocks for multi-functional optics, Light Sci. Appl. 7 (1) (2018).

[54] X. Gao, X. Han, W.-P. Cao, H.O. Li, H.F. Ma, T.J. Cui, Ultrawideband and high-efficiency linear polarization converter based on double V-Shaped metasurface, IEEE Trans. Antennas Propag. 63 (8) (2015) 3522–3530.

[55] J. Ge, Y. Zhang, H. Li, H. Dong, L. Zhang, Ultra-broadband, tunable, and transparent microwave meta-absorber using ITO and water substrate, Adv. Opt. Mater. 11 (10) (2023).

[56] D.R. Smith, D.C. Vier, T. Koschny, C.M. Soukoulis, Electromagnetic parameter retrieval from inhomogeneous metamaterials, Phys. Rev. E 71 (3) (2005).

[57] J. Ren, J.Y. Yin, Cylindrical-water-resonator-based ultra-broadband microwave absorber, Opt. Mater. Express 8 (8) (2018) 2060.

[58] J. Ren, J. Yin, 3D-printed low-cost dielectric-resonator-based ultra-broadband microwave absorber using carbon-loaded acrylonitrile butadiene styrene polymer, Materials 11 (7) (2018) 1249.

[59] Y. Liu, X. Huang, H. Yang, L. Hua, Y. Lei, Zigzag reflective multifunctional metamaterial absorber and polarization rotator with horizontal strip structure, Phys. Scr. 95 (8) (2020) 085510.
[60] Z. Wang, Q. Chen, Y. Ma, T. Guo, C. Shuai, Y. Fu, Design of thermal-switchable absorbing metasurface based on vanadium dioxide, IEEE Antennas Wirel. Propag. Lett. 21 (12) (2022) 2302–2306.
[61] A.G. Hassan, M. Sumaid, F. Ahmed, N. Shoaib, Q.H. Abbasi, S. Nikolaou, Reconfigurable absorptive and polarization conversion metasurface consistent for wide angles of incidence, Sci. Rep. 13 (1) (2023).
[62] S. Li, H. Yang, Y. Yang, Y. Li, X. Huang, A. Zhang, J. Jin, Multifunctional water-based metamaterial with polarization conversion and absorption, Opt. Express 31 (2) (2023) 3336.